Structure-Based Design of a Lead Compound Derived from Natural Schweinfurthins with Antitumor Properties That Target Oxysterol-Binding Protein

Gwenaëlle Jézéquel, Céline Rampal, Carole Guimard, David Kovacs, Joël Polidori, Joëlle Bigay, Jérôme Bignon, Laurie Askenatzis, Marc Litaudon, Alain Pruvost, et al.

Structure-Based Design of a Lead Compound Derived from Natural Schweinfurthins with Antitumor Properties that Target Oxysterol-Binding Protein

Gwenaëlle Jézéquel,† ‡ Céline Rampal,†‡ Carole Guimard,† David Kovacs,† Joël Polidori,# Joëlle Bigay,# Jérôme Bignon,† Laurie Askenatzis,† Marc Litaudon,† Van-Cuong Pham,§ Doan T. M. Huong,§ Anvi Laetitia Nguyen, ¶ Alain Pruvost, ¶ Thierry Virolle,+ Bruno Mesmin,# Sandy Desrat,† Bruno Antonny, # Fanny Roussi†**

† Université Paris-Saclay, CNRS, Institut de Chimie des Substances Naturelles, UPR 2301, 91198 Gif-sur-Yvette, France

Université Côte d'Azur, CNRS, Institut de Pharmacologie Moléculaire et Cellulaire, UMR7275, 06560 Valbonne, France

§ Institute of Marine Biochemistry, Vietnam Academy of Science and Technology, 18 Hoang Quoc Viet, Caugiay, 10000 Hanoi, Vietnam

¶ Université Paris Saclay, CEA, INRAE, Département Médicaments et Technologies pour la Santé (DMTS), SPI, 91191 Gif-sur-Yvette, France

+ Université Côte d'Azur, CNRS, Inserm, Institut de Biologie Valrose, U1091, UMR7277, Parc Valrose, 06000 Nice

KEYWORDS: Schweinfurthins, cholesterol homeostasis, OSBP, prenylated stilbenes, glioblastoma

ABSTRACT

Schweinfurthins (SWs) are naturally occurring prenylated stilbenes with promising anticancer properties. They act through a novel mechanism of action similar to that of other families of natural compounds. Their known target, oxysterol-binding protein (OSBP), plays a crucial role in controlling the intracellular distribution of cholesterol. We synthesized 15 analogues of SWs and demonstrated for the first time that their cytotoxicity as well as that of natural derivatives correlates with their affinity for OSBP. Through this extensive SAR study, we selected one synthetic analogue obtained in one step from SW-G. Using its fluorescence properties, we showed that this compound recapitulates the effect of natural SW-G in cells and confirmed that it leads to cell death via the same mechanism. Finally, after pilot PK experiments, we provided the first evidence of its in vivo efficacy in combination with temozolomide in a patient-derived glioblastoma xenograft model.

INTRODUCTION

Schweinfurthin derivatives (SWs)[1] are prenylated stilbenes isolated from plants of the genus *Macaranga* (Euphorbiaceae), whose first representative, vedelianin **1**,[2] was identified in 1992. Since then, more than twenty analogs (SW A-Q) have been described (Figure 1).[3, 4, 5, 6, 7] Most present a unique hexahydroxanthene (HHX) pattern that endows them with unique cytotoxic properties. Indeed, screening of the NCI 60 human tumor cell lines panel has revealed that their toxicity profile shows little or no resemblance to those of the anti-cancer drugs used in the clinic.[4] The most sensitive cancer cell lines, mainly central nervous system (CNS) cell lines, but also some leukemic, renal, and breast cancer cells, are affected by nanomolar concentrations. In contrast, the less sensitive ones (such as lung, ovarian, and melanoma cancer cells) tolerate micromolar doses. Recent *in vivo* studies revealed that SWs have promising therapeutic potential on a rat chondrosarcoma model[8] and on a murine melanoma model in co-treatment with an anti-PD1.[9] Moreover, the COMPARE algorithm of the NCI has demonstrated that the SWs family has a comparable cytotoxic profile to that of other families of natural compounds (stelletin E,[10] cephalostatin I,[11] and OSW-1[12]), suggesting that they all act *via* a similar mode of action, although not fully understood.

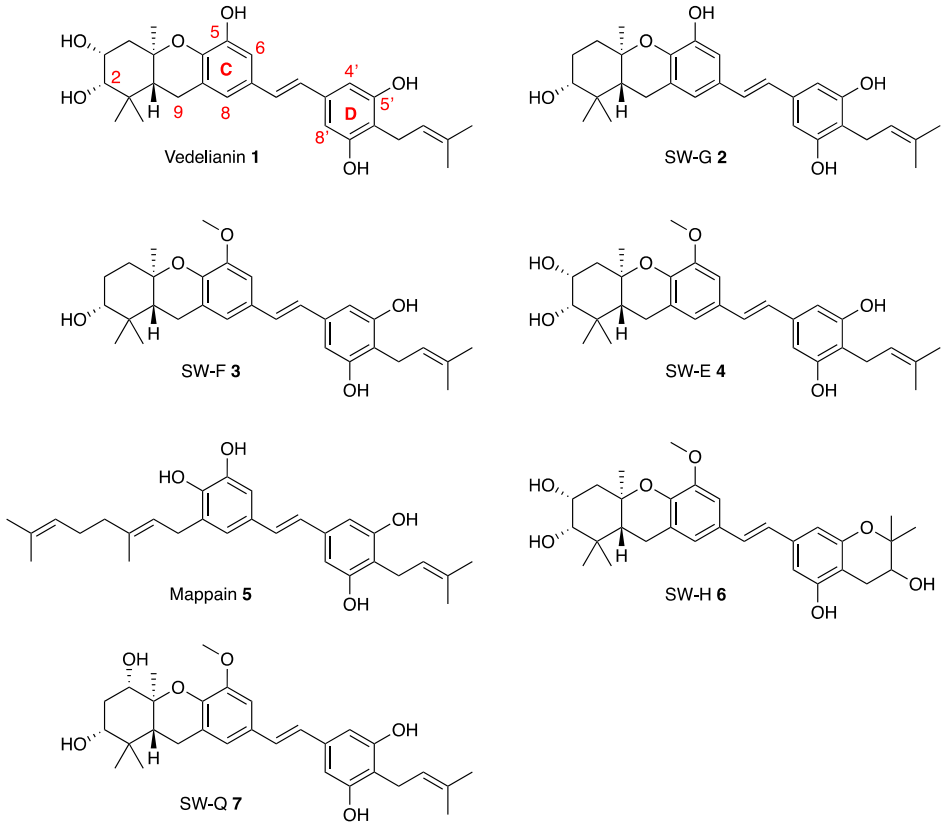

Figure 1. Chemical structures of selected natural schweinfurthin derivatives **1-7**

Ten years ago, Burgett *et al.* identified oxysterol-binding protein (OSBP) as a common intracellular target for these different families of natural molecules.[13] However, they did not precisely characterize their binding mode. Additionally, the role of OSBP in cell death still remains poorly understood, and it is feasible that next to OSBP, other proteins are also efficacy targets of SWs. OSBP and related protein homolog ORPs constitute a family of lipid-transfer proteins (LTPs) that operate at membrane contact sites.[14] OSBP transfers cholesterol from the endoplasmic reticulum (ER) to the trans-Golgi network (TGN), and conversely exchanges phosphatidylinositol 4-phosphate (PI4P) from the TGN to the ER.[15, 16] This protein is a crucial player in controlling intracellular cholesterol distribution as it transports one-third of the cholesterol pool of the cell. Cholesterol and PI4P bind into the OSBP lipid-binding cavity (ORD domain) in a mutually exclusive manner.

By exploiting the intrinsic fluorescence of its stilbene moiety, we have recently shown that SW-G **2** perfectly colocalized with OSBP in the cell. [17] We have also determined that this compound specifically inhibited the lipid exchange cycle of OSBP with an apparent *Ki* < 1 nM by direct binding into its ORD domain. Moreover, we have demonstrated that, in cells, the interaction between SW-G **2** and OSBP reduced PI4P turnover as well as membrane cholesterol levels and delayed post-Golgi trafficking.**Erreur ! Signet non défini.** It has been reported that delayed post-Golgi trafficking induces ER stress, suppresses both PI3K activation and mTOR/ RheB complex formation and subsequently leads to the inhibition of PI3K/AKT/mTOR signaling.[18] Since these signaling events can lead to apoptosis, these results have added to the understanding of the mode of action of SWs and created a link between OSBP and cell death. [18]

Despite their therapeutic interest, the study of SWs has been hampered so far because they were isolated with low yield from *Macaranga* species and/or could be synthesized in 5% maximum overall yield in 16 to 20 steps by an elegant but poorly divergent strategy.[19] Nevertheless, several analogs were developed by this approach to establish structure-activity relationships. These SARs were all based on the cytotoxicity of these compounds either on the 60 cell-lines assay of the NCI or on a more straightforward two-cell assay (one cell line sensitive; to the SWs, another more resistant).[20, 21] Both strategies have shown that the HHX moiety, one phenol on the D-ring, and the *trans*-stilbene motif are mandatory to keep the cytotoxic profile of SWs even if this latter can, to some extent, be replaced by an amide[22] or triazole ring.[23] On the contrary, some portions of the molecule are tolerant to modifications (the prenyl chain and one phenol on the D-ring, for example).

Until now, the affinity of SW derivatives for OSBP has never been assessed, which has prevented a correlation between affinity for OSBP and the specific cytotoxic profile. In this publication, we present, for the first time, a systematic and extensive evaluation of the affinity of new and known SW analogs for

OSBP, which we compared with their cytotoxic activity. This analysis enabled us to select one compound as a new lead and to provide the first proof of *in vivo* efficacy of SWs derivatives on a glioblastoma model. We focused on this model because SWs are highly cytotoxic on CNS lines (such as U-87 MG) and because it is a cancer with a very poor prognosis for which new effective therapeutic approaches are strongly expected.

RESULTS AND DISCUSSION

Chemistry. A few years ago, we disclosed a new isolation process for SWs based on innovative metabolomic studies and mass spectrometry imaging.[24, 25] Consequently, vedelianin **1**, SW-G **2**, SW-F **3**, and SW-E **4** can be isolated at the gram scale. This new process facilitated the synthesis of various analogues by late-stage functionalization. This allowed us to revisit and strengthen the already known SAR studies based on the affinity of these compounds for OSBP.

First, we performed chemical modifications on ring C (Scheme 1). Thus, we carried out Williamson reactions on SW-G **2** in the presence of either propargyl or allyl bromide to obtain compounds **8** and **9**, extending the exploration of the functionalization at C-5.[26] Sodium hydride was chosen as the base as it gave better yields than K_2CO_3 without forming the alkylated product on the hydroxyl at C-2. Thus, with 1.1 equivalents of NaH and 1.2 equivalents of alkyl bromide, the C-5 functionalized compounds **8** and **9** were almost exclusively formed. This regioselectivity was confirmed by analysis of their ^{1}H NMR spectra since, in both cases, the H-4' and H-8' protons adjacent to the phenols at C-5' and C-7' had the same chemical shift (at δ_H 6.52). When one of the phenols on ring D is functionalized, the chemical shifts of the H-4' and H-8' protons are different due to a desymmetrization of this part of the molecule. From aryl propargyl ether **8**, a selective cyclo-isomerization was undertaken using Gagosz's catalyst to give 2*H*-chromene **10** functionalized at C-5 and C-6.[27] From aryl allyl ether **9**, a Claisen rearrangement[28] enabled the formation of the SW-G analog **11** functionalized at C-6 (Scheme 1). This regioselectivity was established by analyzing the 1D and 2D NMR spectra of the formed product, in particular thanks to an HMBC correlation from H-8 (at δ_H 7.92) to C-9 (at δ_c 22.9).

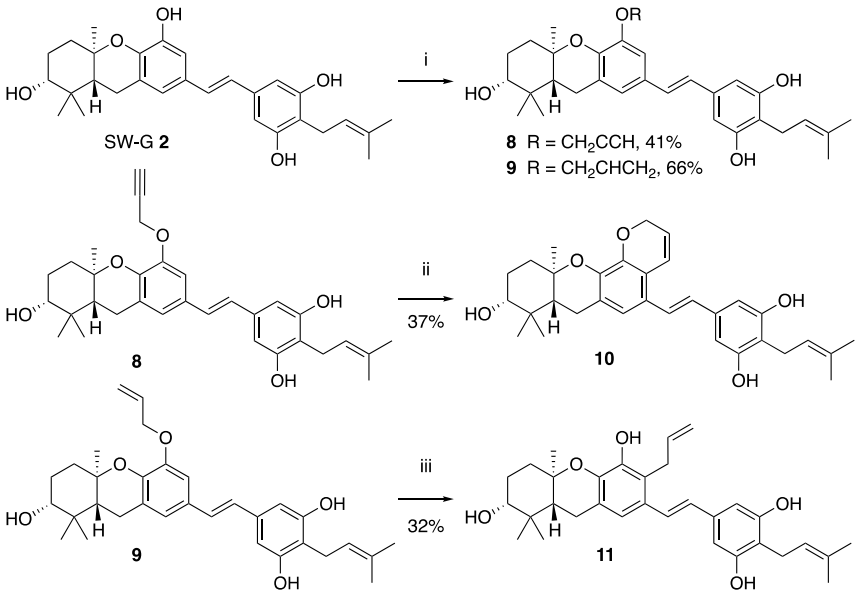

Scheme 1. Synthetic route to compounds **8**-**11** modified on ring C. Reagents and conditions: (i) NaH, DMF, 0 °C, 15 min then $BrCH_2R$, 0 °C or r.t., 5h30; (ii) $Ph_3PAuNTf_2$, DCM, r.t., 2 h; (iii) DMF, 150 °C, 10h.

Next, we modified ring D (Scheme 2). Starting from SW-G **2**, SW-F **3**, and SW-E **4**, we could elaborate, in one step, chromane derivatives **12**-**14** by simple stirring at room temperature in formic acid, which resulted in the cyclization of one of the phenols of ring D on the prenyl chain and concomitant formylation of the alcohol of the HHX. In addition, performing the same reaction in the presence of a catalytic amount of Pd_2dba_3, a source of Pd(0), enabled us to complete the reduction of the double bond of the stilbene simultaneously.[29] The formyl ester could easily be removed using standard conditions to yield compounds **15**-**17** and **20-21** (Scheme 2).

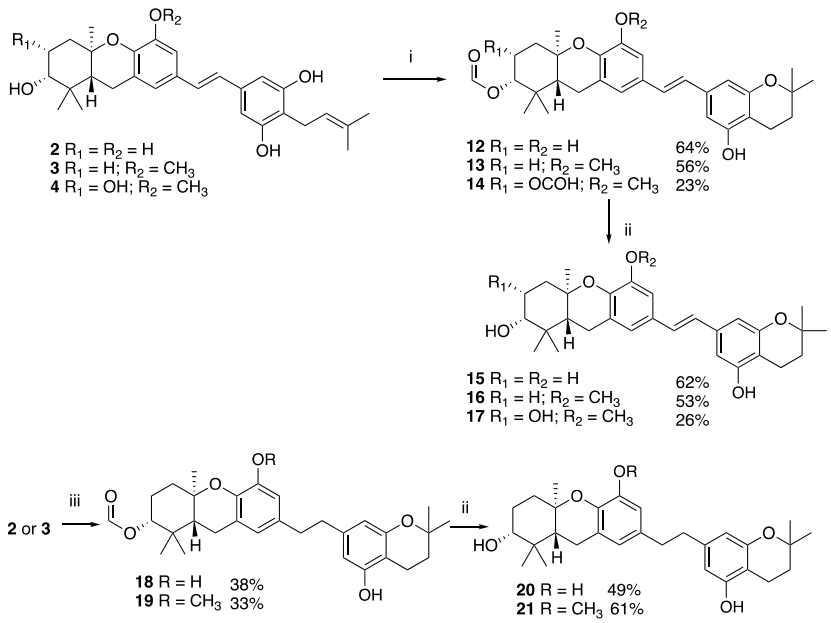

Scheme 2. Synthetic route to compounds **12**-**22** cyclized on ring D. Reagents and conditions: (i) Pd_2dba_3, NaOAc, HCO_2H, r.t., 4 h; (ii) LiOH, THF/H_2O, r.t., 1 h; (iii) Pd_2dba_3, NaOAc, HCO_2H, r.t., 18 h.

Biochemical Evaluation. We evaluated the affinity for OSBP of compounds **1-21** and determined in parallel their cytotoxicity on two cancer cell lines: U-87 MG glioblastoma cells, which are highly sensitive to SWs, and A549 lung cancer cells, which are more resistant (Table 1). To determine the affinity of each compound for OSBP, we evaluated its ability to inhibit cholesterol transport using *in vitro* liposome-based reconstitution experiments.[Erreur ! Signet non défini.] Specifically, we followed in real time the transfer of dehydroergosterol (DHE) by the ORD domain of OSBP between two liposome populations in the presence or the absence of each compound. The donor liposomes (LE) mimicked the ER and contained DHE, a fluorescent analog of cholesterol. The acceptor liposomes mimicked the Golgi (LG) and contained the fluorescent lipid dansyl PE. Transport of DHE from the donor to the acceptor liposomes was accompanied by a FRET signal between DHE and Dansyl-PE, enabling accurate kinetics measurements. Each compound was tested at eight concentrations, allowing us to determine an apparent inhibitory constant (K*i*) for OSBP (see experimental section).

Table 1. Effects of compounds **1**-**21** on the inhibition of cholesterol transfer and cytotoxicity on two cell lines

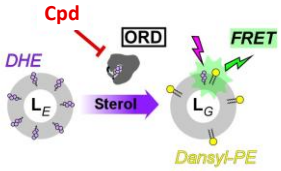

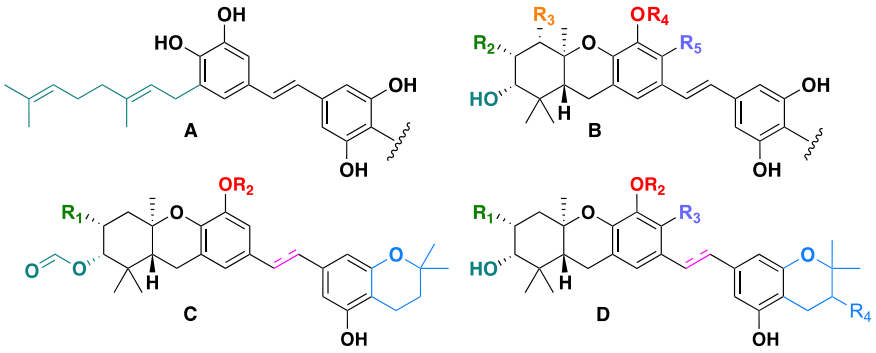

Compound	Series	OSBP [a]	U-87 MG [b]	A549 [b]
		Ki (nM)	IC_{50} (nM)	
Vedelianin **1**	B	< 1	15 ± 0.55	966 ± 15
SW-G **2**	B	< 1	8 ± 0.4	359 ± 26
SW-F **3**	B	6	98 ± 3	605 ± 37
SW-E **4**	B	< 1	22 ± 2.6	397 ± 15
Mappain **5**	A	3000	7000 ± 400	>10000
SW-H **6**	D	401	656 ± 31	1793 ± 92
SW-Q **7**	B	254	510 ± 23	1115 ± 56
8	B	43	286 ± 14	3901 ± 195
9	B	31	420 ± 21	5002 ± 350
10	B	37	481 ± 19	> 10000
11	B	119	457 ± 21	2855 ± 145
12	C	1070	12.4 ± 3.3	733 ± 58
13	C	523	380 ± 18	2421 ± 85
14	C	829	500 ± 38	2147 ± 112
15	D	< 1	9.4 ± 0.14	647 ± 62
16	D	64	478 ± 26	2533 ± 140
17	D	16	336 ± 16	1095 ± 61

18	C	3224	67 ± 2.1	3040 ± 200
19	C	3701	1485 ± 368	> 10000
20	D	< 1	77 ± 1.98	3910 ± 536
21	D	46	3850 ± 421	> 10000

[a]Inhibitory effect of the indicated compounds on DHE transfer mediated by OSBP ORD domain. The K*i* of each compound was calculated after three independent experiments, using either a quadratic (for potent inhibitors) or a hyperbolic equation (for weak inhibitors); [b]IC_{50} measures the drug concentration required for the inhibition of 50% cell proliferation after 72 h of incubation and was calculated from three independent experiments.

We observed a very good parallel between K*i* for OSBP and cytotoxicity on U-87 MG. Compounds with a very high affinity for OSBP (< 1 nM) like **1**, **2**, **4**, and **15** showed cytotoxicity on U-87 MG below 20 nM except **20**, which had an IC_{50} of 77 nM. Compounds **3**, **8**-**11**, **16**, **17** and **21**, with a good affinity (from 2 to 200 nM), presented cytotoxicity below 500 nM. Compounds **5**, **6** and **7** with a weak (from 200 to 2000 nM) or a very weak affinity (above 2000 nM) were less cytotoxic or not cytotoxic at all. In addition, all compounds showed lower cytotoxicity for A549 cells, which ranged from 359 nM to > 10 μM.

However, we noticed that compounds of the C series, *i.e.,* **12**-**14** and **18** -**19**, which carry formate on the alcohol of the HHX unit, behave differently: these compounds were poorly inhibitory for OSBP *in vitro*, but their cytotoxicity was similar to that of their non-esterified counterpart **15**-**17** and **20**-**21**. We hypothesized that this uncommon ester was hydrolyzed in cells, indicating that compounds **12**-**14** and **18**-**19** may be prodrugs of **15**-**17** and **20**-**21**.

Altogether, these biochemical assessments clarify most of the SARs previously established by Wiemer *et al.* but also temper some of their results. As previously demonstrated, the HHX moiety is necessary for biological activity as nontoxic mappain **5** (A series) did not bind the ORD domain of OSBP. Secondly, the presence of hydroxyl at C-3 on the HHX unit improves the affinity for OSBP. Thus, if vedelianin **1** and SW-G **2** have a high affinity for OSBP, SW-F **3** is less active than SW-E **4** (6 nM *vs.* < 1 nM). In contrast, a hydroxyl on C-4 is highly detrimental (see compound **7**, which presents an affinity of 254 nM for OSBP).

As already described,[26] an ether function at C-5 decreases the affinity for OSBP (see SW-F **3** or compounds **8** and **9** with an affinity of 6, 43, and 31 nM, respectively). The more crowded the alkyl group, the lower the affinity for OSBP. Nevertheless, SW-E **4** with two hydroxyls on the HHX is as potent as vedelianin **1** and SW-G **2** (< 1 nM). The affinity decrease is the same when C-6 is alkylated (see compounds **10** and **11**).

Moreover, modification of the eastern part of the molecule significantly impacts activity. Overall, the formation of a chromane was slightly detrimental, as already published for a benzofuran or hydroxybenzofuran,[21] except compound **15,** which was as active as compound **2**. In addition, when the chromane was functionalized with a hydroxyl group, the bioactivity decreased drastically: natural SW-H **6** (401 nM) was thus 25 times less active on OSBP than unfunctionalized compound **17** (16 nM), which was, itself, 16 times less active than uncyclized compound **4** (< 1 nM). In contrast to published results,[21] reduction of the double bond of the stilbene had no impact on the OSBP inhibition (see compounds **20** and **21** *vs.* compounds **15** and **16** respectively).

From this comprehensive series of *in vitro* and *in vivo* tests, we selected compound **12** for further investigation as it was obtained with a good yield in one step from SW-G **2** and may be the prodrug of compound **15**, which was very active on OSBP *in vitro* and as cytotoxic as SW-G **2**.

Cellular validation. We first tracked the fate and the effect of compound **12** in the cell compared to SW-G **2** (Figure 2). First, we took advantage of the fluorescence properties of these two stilbenes, which exhibit excitation and emission peaks at 330 and 410 nm, to visualize them directly in RPE-1 cells using an imaging system adapted to UV.[Erreur ! Signet non défini.] After 30 min of incubation with **12** or SW-G **2**, RPE-1 cells were fixed, permeabilized and further processed for immunofluorescence using antibodies against OSBP and a TGN marker. In this experiment, compound **12**, like SW-G **2,** accumulated mainly in the perinuclear region and colocalized with OSBP, confirming OSBP as its intracellular target (Figure 2-A). Next, we studied the influence of compounds **12** and **2** on the lipid exchange activity of OSBP in cells, focusing on the intracellular distribution of PI4P, which is exchanged for cholesterol at the ER-TGN interface (Figure 2-B). For that, we used RPE-1 cells stably expressing the GFP-P4M^{SidM} construct, which acts as a PI4P-specific fluorescent probe that can be detected by video microscopy.[30, 16] Owing to its well-developed TGN, this cell line is well adapted to imaging studies of molecular processes occurring in this organelle.

GFP-P4M^{SidM} showed a cytosolic distribution in untreated cells with a slight enrichment at the TGN (Figure 2-C; t=0). After the addition of **2** or **12**, the fluorescence of the GFP-P4M probe became much stronger at the TGN, indicating an increase in PI4P at the TGN following OSBP inhibition. Interestingly, a time shift in the response of the PI4P probe was noted depending on the compound: the probe accumulated at the TGN slower with compound **12** ($t_{1/2}$ = 25 min) than with **2** ($t_{1/2}$ = 10 min). Next, we used confocal microscopy to compare the effect of compound **12** to that of SW-G **2** on endogenous OSBP. Consistent with the inhibition of PI4P transfer by OSBP, both compounds promoted OSBP recruitment to the TGN 10 min after treatment (Figure 2-C). We also noted that a partial fragmentation

of the Golgi followed this effect after 4 h and concomitant fading of the OSBP signal at the TGN. Altogether, these observations demonstrate that compound **12**, like compound **2,** is effective at blocking PI4P turnover at the TGN, confirming that compound **12** acts, like SW-G **2**, as a potent OSBP inhibitor in a cellular context. Furthermore, the difference in P4M recruitment kinetics suggests that compound **12** requires preliminary processing in the cell to be active (*i.e*., cleavage of the ester of the HHX motif by nonspecific esterases), supporting the idea that it acts as a prodrug.

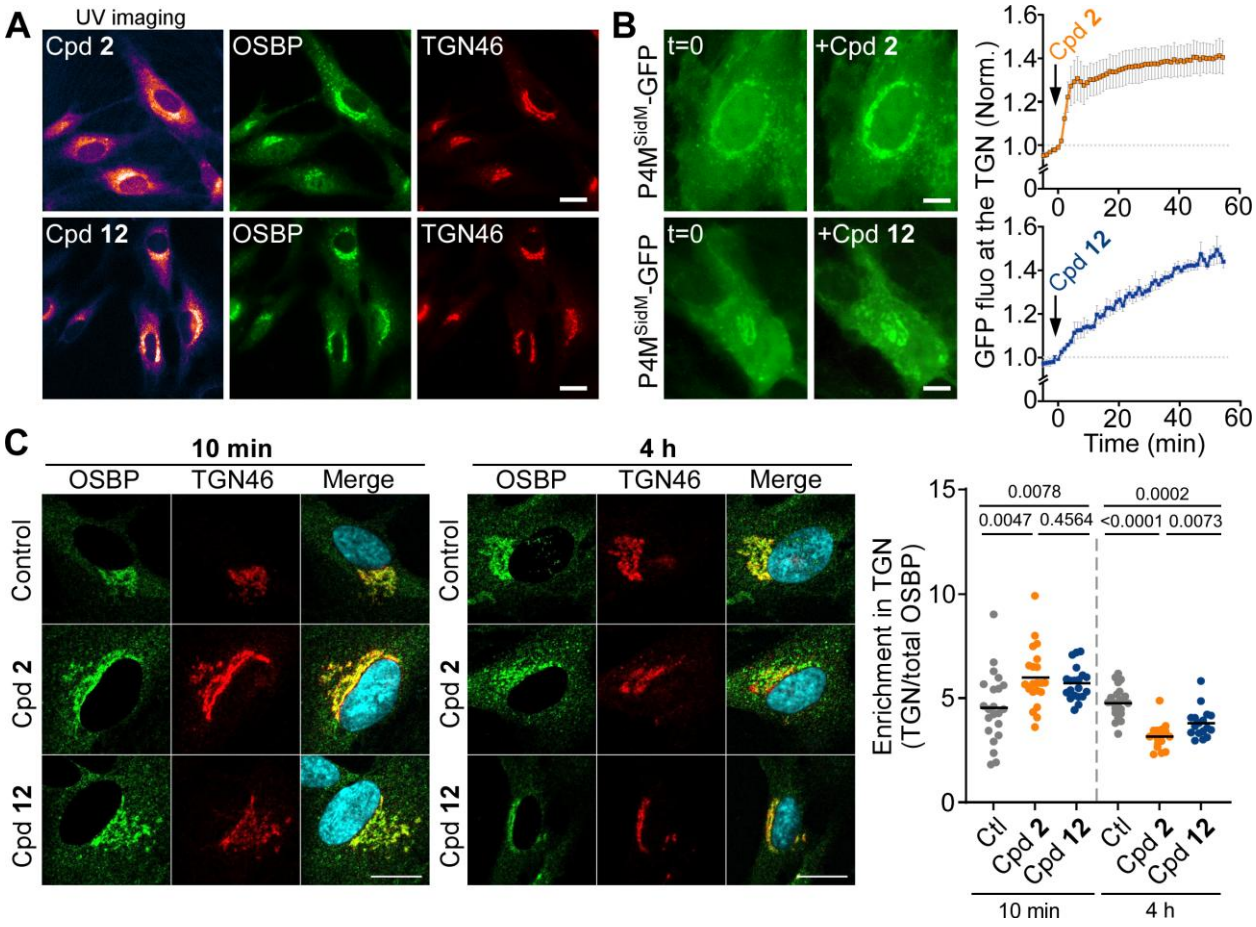

Figure 2. A- Direct widefield fluorescence imaging of compound **12** and SW-G **2** in RPE-1 cells after 30 min of incubation, fixation, permeabilization, and immuno-labeling to assess the localization of endogenous OSBP and TGN-46. **B-** Timelapse imaging of RPE-1 cells expressing P4M-GFP upon addition of SW-G **2** or compound **12**. Left: images of cells before and 50 min after the addition of the compounds. Right: graphs showing P4M-GFP fluorescence intensity at the TGN over time. Results are mean of 4 to 6 independent experiments ± SEM. **C-** Confocal images of RPE-1 cells treated or not with SW-G **2** or **12**, after fixation, permeabilization, and immunolabeling with anti-TGN46 and anti-OSBP. Right: OSBP intensity ratio (TGN/Total OSBP) from n = 17–24 measurements for each condition.

Last, we determined the impact of compound **12** on mTOR signaling (Figure 3). As Bao *et al.* have shown that SW-G **2** impacts mTOR signaling, which inhibition was potentially responsible for cell death,[Erreur ! Signet non défini.] we checked whether the effect of compound **12** was similar. As shown in Figure 3, phosphorylation of ribosomal protein S6 Kinase 1 (S6K) and S6 protein downstream of mTORC1 and that of AKT protein on Ser 473 downstream of mTORC2 was inhibited in a dose-dependent manner after treatment with compounds **2** and **12**, confirming that the mTOR pathway is impacted.[Erreur ! Signet non défini.] Moreover, a dose-dependent decrease of LC3I in favor of LC3II formation, as well as degradation of P62 protein, accounted for a subsequent autophagy process.[31]

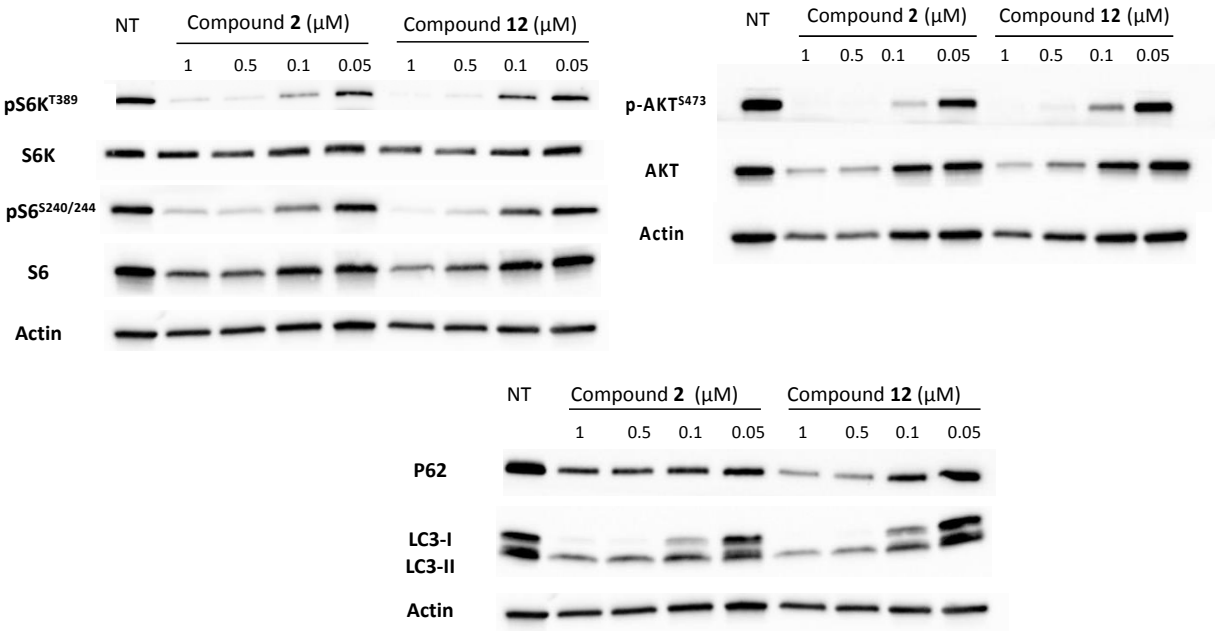

Figure 3. Effects of compounds **2** and **12** on the mTorC1 (A), mTorC2 (B) and autophagy (C) pathways monitored by western blot analysis performed on U-87 MG after 48 h incubation with increasing doses of **2** and **12**. The actin level served as a protein loading control.

Stability and pilot pharmacokinetic studies. We performed stability measurements in mouse plasma and microsomes to determine if compounds **2**, **15**, and **12** (assumed prodrug of **15**) are stable in physiologic media. In particular, mouse liver microsomes are useful *in vitro* hepatic clearance models as they contain many drug-metabolizing enzymes of the liver, which is the main organ for drug metabolism. Only SW-G **2** and compound **15** were stable in mouse plasma (Table 2). In contrast, compound **12** was transformed into compound **15** in about 100 minutes. As for microsomal stability, compound **15** was the only one that presented good *in vitro* intrinsic clearance, *i.e.*, < 48 µL/min/mg protein, whereas SW-G **2** and compound **12** were promptly metabolized by hepatic enzymes and had a high clearance (90 and 120 µL/min/mg protein respectively).

Table 2. In vitro stability assays

***In vitro* mouse plasma stability**

Compound	**2**	**12**	**15**
Metabolic stability (%) t = 120 min	100	20.2	100
Half-life (min)	-	51	-
Metabolite(s)	-	**15**	-

***In vitro* mouse microsomal stability**

Compound	**2**	**12**	**15**
Metabolic stability (%) t = 45 min	23	5.3	48.6
In vitro intrinsic clearance (µL/min/mg protein)	90	120	32
Metabolic stability (%) non-NADPH dependent	100	16	100

We then performed an early screening test to estimate plasma concentrations of compounds **12** and **15** after intraperitoneal single administration of compound **12** at two doses (5 mg/kg and 20 mg/kg) in Swiss mice (Figure 4). For that, a 2.5 mg/mL solution of compound **12** was administrated to two groups of three mice whose blood was collected at six different times. After plasma recovery and protein precipitation, the dosage of both compounds was carried out using LC-MS/MS. The obtained results indicated that Cmax and AUC were linear (5 mg/kg *vs.* 20 mg/kg) and the metabolization of compound **12** to compound **15** was fast. At 20 mg/kg, the plasma ½ life of compound **15** was around 2 h and plasma concentration in compound **15** was higher than 300 ng/mL (600 nM) for 3 h (*i.e.,* well above the IC_{50} of **15** on a sensitive line like U-87).

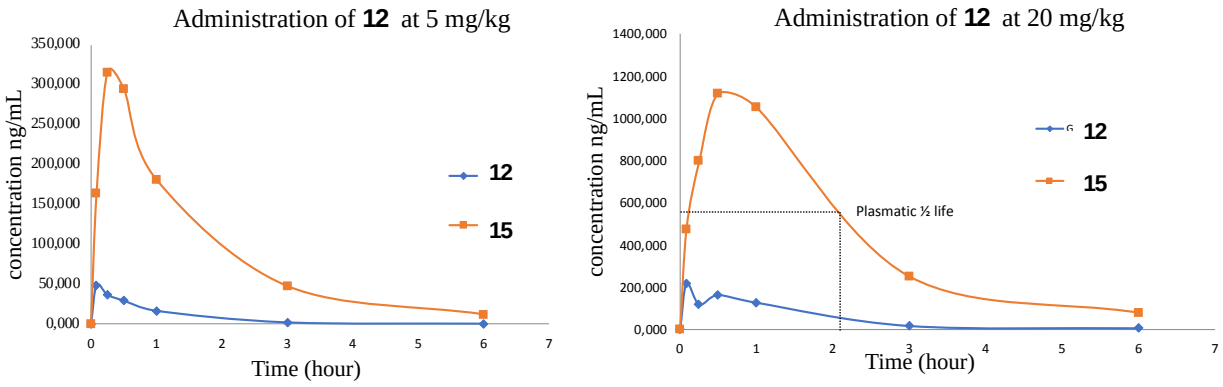

Figure 4. Mean plasma concentrations of compounds **12** and **15** after intraperitoneal administration of compound **12** in Swiss mice at 5 mg/kg (left panel) and 20 mg/kg (right panel).

***In vivo* evaluation.** As SWs are highly cytotoxic on CNS lines, such as U-87 MG, we validated the *in vivo* efficacy of compound **12** on a glioblastoma (GBM) model. GBM is the most common form of primary brain tumour afflicting adult patients of all ages. It is a highly vascularized and fast-growing tumour characterized by a heterogeneous population of genetically unstable cells. Because of its infiltrative nature and the risk of damage to adjacent healthy tissue, complete surgical resection of the tumour is impossible. The current therapy relies thus on surgery, radiotherapy and adjuvant chemotherapy with temozolomide (TMZ). TMZ is an oral alkylating agent that kills cancer cells via guanine/adenine methylation-mediated DNA base pair mismatches and subsequent DNA damage-induced reactive oxygen species (ROS) accumulation. Nevertheless, GBM often develops resistance to current therapies and leads to a fatal outcome with a median survival of only 12−15 months. Thus, alternative therapeutic approaches are highly needed. [32]

As a first step, we determined that compound **12** was nontoxic at 100 mg/kg administrated once a day for 5 consecutive days to non-tumor bearing immunodeficient mice. This low toxicity allowed us to consider the administration of compound **12** at a dose of 20 and 50 mg/kg as a single agent or in combination with temozolomide in the GBM1-HAM patient-derived glioblastoma xenograft model developed in immunodeficient female mice. This study consisted of 5 groups of 10 mice each: vehicle (group 1), compound **12** at 50 mg/kg i.p. (group 2), and temozolomide at 42 mg/kg p.o. (group 3), compound **12** at 50 mg/kg in combination with temozolomide at 42 mg/kg (group 4), and compound **12** at 20 mg/kg in combination with temozolomide at 42 mg/kg (group 5) (Figure 5).

Based on body weight data and clinical observations, all tested compounds used as monotherapy or in combination were tolerated. However, slight and transient bodyweight losses and some clinical signs

were reported in the compound **12**/temozolomide combination groups irrespective of **12** dosing (50 or 20 mg/kg). Compound **12** (group 2) and temozolomide (group 3), each administered as a single agent, induced modest but statistically significant tumor growth inhibition compared to the control group: $p < 0.01$ from D7 to D11, with TGDI = 1.37, T/C and best T/C = 70.05% and ΔT/T0 = 625.61% at the control group day end D11 in group 2 and $p < 0.01$ from D9 to D11, with TGDI = 1.34, T/C and best T/C = 62.43% and ΔT/T0 = 546.69% at the control group day end D11 in group 3. The combination of **12** and temozolomide demonstrated statistically significant potentiation of antitumor activity over each compound used in monotherapy. In group 4, we observed a moderate and statistically substantial slowdown of tumor growth compared to a control group ($p < 0.01$ on D7 and $p < 0.001$ from D9 to D11), with TGDI = 2.07, T/C and best T/C = 41.43% and ΔT/T0 = 329.18% at the control group day end D11. Tumor growth inhibition by this combination was also statistically higher than by **12** alone ($p < 0.001$) or temozolomide alone ($p < 0.05$). The degree of tumor growth inhibition was more significant than in group 5 with a lower dose of **12**, which showed a TGDI of 1.75, T/C and best T/C = 49.91% and ΔT/T0 = 396.24% at the control group day end D11.

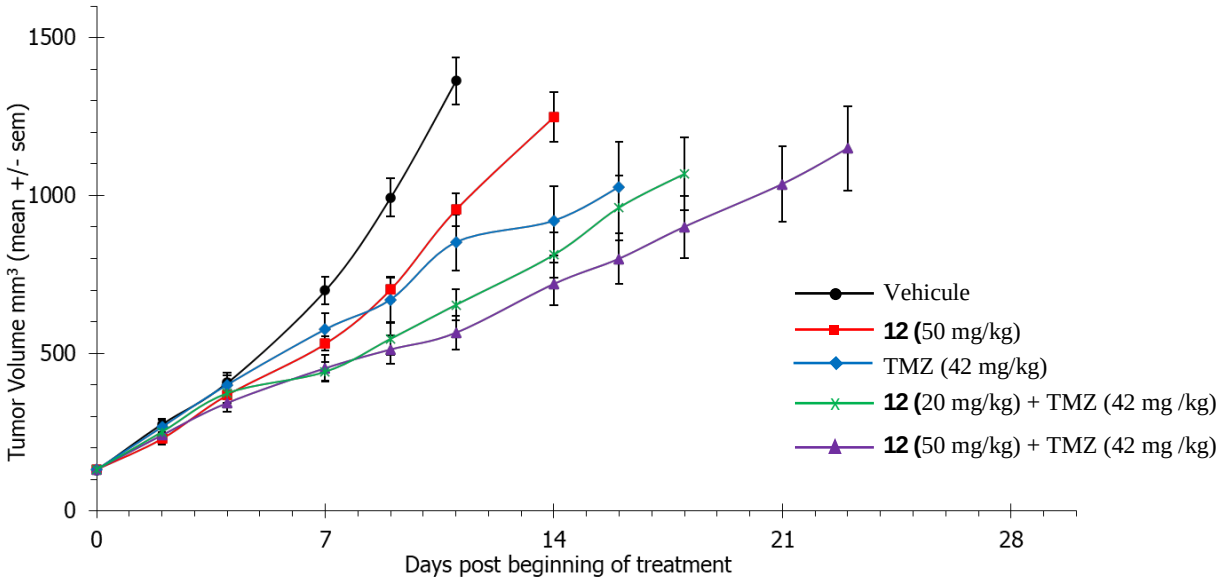

Figure 5. *In vivo* experiments on a GBM1-HAM patient-derived glioblastoma xenograft model developed in immunodeficient female mice. It consisted of 5 groups of 10 mice each: vehicle, compound **12** at 50 mg/kg i.p., temozolomide at 42 mg/kg p.o., compound **12** at 50 mg/kg in combination with temozolomide at 42 mg/kg, and compound **12** at 20 mg/kg, in combination with temozolomide at 42 mg/kg.

Finally, complementary preliminary experiments conducted to evaluate the ability of compound **15** to pass through the blood-brain barrier after intraperitoneal administration of compound **12** indicated that the brain/plasma ratio of compound **15** was 1.74 ± 0.27 after 1.5 h, demonstrating the ability of these molecules to cross efficiently the blood-brain barrier.

CONCLUSION

In a few steps from natural SWs, we have elaborated fifteen new derivatives **8**-**21** via a late-stage approach. For the first time, we have established, *in vitro*, that the toxicity profile of these compounds and that of natural SWs **1**-**7** correlates with their affinity for the ORD domain of OSBP, strongly suggesting that OSBP has a crucial role in the mode of action of SWs. Moreover, we have shown that new compound **12** recapitulates the effect of SW-G **2** on both OSBP in cells and the mTOR pathway. Compound **12** is a prodrug of compound **15** that, unlike SW-G, has a good *in vitro* intrinsic clearance. Finally, we provide the first proof of the *in vivo* efficacy of compound **12** in combination with temozolomide in a patient-derived glioblastoma xenograft model. We conclude that SW derivatives are promising anti-cancer compounds that deserve further development and characterization.

EXPERIMENTAL SECTION

Plant Material. The green fruits of *M. tanarius* were collected in June 2014 at A Luoi, Thua Thien Hue Province, Vietnam, and authenticated by N.T. Cuong and D.D. Cuong. A voucher specimen (VN-2371) has been deposited at the Herbarium of the Institute of Ecology and Biological Resources of The Vietnam Academy of Science and Technology, Hanoi, Vietnam. ABS-CH Unique Identifier (UID): ABSCH-IRCC-VN-255602-1.

Extraction and Isolation. The isolation of compounds **1** to **7** has already been described in previous articles.[7, 24]

Chemistry. All reagents and solvents were used as purchased from commercial suppliers or were purified/dried according to Armarego and Chai.[33] Purifications by column chromatography on silica gel were performed using Merck Silica Gel 60 (70–230 mesh). ^{1}H and ^{13}C NMR spectra were recorded on Bruker ARX500 instruments using $CDCl_3$ or CD_3CN as internal reference. Chemical shifts (δ values) are given in parts per million (ppm), and the multiplicity of signals are reported as follows: s, singlet; bs, broad singlet; d, doublet; t, triplet; q, quartet; dd, doublet of doublets; m, multiplet. HRMS analyses were performed using a Waters LCT Premier instrument by ElectroSpray Ionization (ESI). All compounds

are >95% pure by UPLC analysis performed on a Waters Acquity TQD instrument using a BEH C18 column 2.1 x 50 mm and a gradient of water/acetonitrile from 95:5 to 0:100.

Procedure A. General procedure for alkylation of schweinfurthins. To a solution of SW-G **2** or compound **12**, in anhydrous DMF (1 mL for 0.1 mmol) at -15 °C, was added dropwise a suspension of NaH (1.1 eq) in anhydrous DMF. After 15 min, propargyl bromide or allyl bromide (1.2 eq) was added, and the mixture was stirred for 5 h 30 at 0 °C. A saturated solution of NH_4Cl was added and the products were extracted with EtOAc (3 times). The combined organic phases were dried over $MgSO_4$ and concentrated under reduced pressure. The crude mixture was then purified by flash chromatography on silica gel to afford the pure product.

Procedure B. General Procedure for Gold Cyclisation from Propargyl Derivatives. To a solution of SW derivative in anhydrous CH_2Cl_2 (1 mL for 0.04 mmol), was added Gagosz catalyst (PPh_3AuNtf_2, 0.01 eq). The resulting orange solution was stirred at r.t. under argon for 2 h, then concentrated under reduced pressure. The crude mixture was purified on preparative TLC plates of silica gel using heptane/acetone 1:1 to obtain the pure desired product.

Procedure C. General procedure for intramolecular cyclisation using formic acid. SW derivatives were stirred in formic acid (1 mL for 0.3 mmol) under argon at room temperature for 5 h. After addition of CH_2Cl_2 (2 mL), the organic phase was decanted washed successively twice with water, a saturated solution of $NaHCO_3$ and brine. The organic phase was dried over $MgSO_4$ and concentrated under reduced pressure. The crude mixture was then purified by flash chromatography on silica gel to afford the pure product.

Procedure D. General procedure for intramolecular cyclisation and reduction using tris (dibenzylideneacetone) dipalladium (0) and formic acid. SW derivatives were stirred in formic acid (1 mL for 0.3 mmol) with Pd_2dba_3 (0.02 eq) and NaOAc (0.3 eq) under argon at room temperature for 24 h. After addition of CH_2Cl_2 (2 mL), the organic phase was decanted washed successively twice with water, a saturated solution of $NaHCO_3$ and brine. The organic phase was dried over $MgSO_4$ and concentrated under reduced pressure. The crude mixture was then purified by flash chromatography on silica gel to afford the pure product.

Procedure E. General procedure for hydrolysis of formate esters using LiOH. To a solution of formate ester in THF (1 mL for 0.1 mmol), was added a solution of $LiOH.H_2O$ (2.5 eq) in H_2O. The resulting brownish solution was stirred at r.t. for 1h. After addition of a HCl 1 N solution, the crude mixture was

extracted with EtOAc (3 times). The combined organic phases were dried over $MgSO_4$ and concentrated under reduced pressure. The crude mixture was purified by flash chromatography on silica gel or on a preparative TLC to afford the pure product.

5-((*E*)-2-((2*R*,4a*R*,9a*R*)-2-hydroxy-1,1,4a-trimethyl-5-(prop-2-yn-1-yloxy)-2,3,4,4a,9,9a-hexahydro-1H-xanthen-7-yl) vinyl)-2-(4-methylpent-3-en-1-yl) benzene-1,3-diol (**8**). Following procedure A, compound **8** (88 mg) was obtained with 41% yield from SW-G **2** (198 mg). ^{1}H NMR (CD_3CN, 500MHz) δ 0.83 (s, 3H), 1.05 (s, 3H), 1.19 (s, 3H), 1.59 (m, 1H), 1.66 (s, 3H), 1.66 (m, 1H), 1.72 (m, 1H), 1.74 (s, 3H), 1.75 (m, 1H), 1.98 (m, 1H), 2.73 (m, 2H), 2.77 (d, 1H, *J* = 5.3 Hz, OH), 2.79 (t, 1H, J = 2.2 Hz), 3.33 (s, 1H), 3.25 (d, 2H, *J* = 7.1 Hz), 4.74 (d, 2H, *J* = 2.2 Hz), 5.17 (t, 1H, *J* = 7.1 Hz), 6.52 (s, 2H), 6.84 (d, 1H, *J* = 16.6 Hz), 6.91 (d, 1H, *J* = 16.6 Hz), 6.93 (d, 1H, *J* = 1.5 Hz), 7.02 (d, 1H, *J* = 1.5 Hz,), OH5' and OH7' signals are missing. ^{13}C NMR (CD_3CN, 125 MHz) δ 14.9, 18.0, 20.3, 23.0, 23.8, 25.9, 27.7, 28.9, 38.6, 39.1, 47.8, 57.4, 76.8, 77.8, 78.2, 80.0, 106.0 (2 C), 111.2, 115.2, 123.0, 123.8, 124.7, 127.2, 128.5, 129.8, 132.2, 137.4, 144.3, 147.6, 156.8 (2 C). HRMS (ESI): *m/z* calculated for $C_{32}H_{39}O_5^+$ [M+H]$^+$: 503.2792; found: 503.2798. $[\alpha]_D^{24}$ (*c* 1.0, MeOH) = + 80°.

5-((*E*)-2-((2*R*,4a*R*,9a*R*)-5-(allyloxy)-2-hydroxy-1,1,4a-trimethyl-2,3,4,4a,9,9a-hexahydro-1H-xanthen-7-yl) vinyl)-2-(4-methylpent-3-en-1-yl) benzene-1,3-diol (**9**). Following procedure A, compound **9** (143 mg) was obtained with 66% yield from SW-G **2** (190 mg). ^{1}H NMR ($CDCl_3$, 500 MHz) □ 0.86 (s, 3H), 1.08 (s, 3H), 1.24 (s, 3H), 1.59 (m, 1H), 1.69 (m, 1H), 1.75 (s, 3H), 1.81 (s, 3H), 1.82 (m, 1H), 1.84 (m, 1H), 2.07 (m, 1H), 2.70 (m, 2H), 3.40 (m, 3H), 4.61 (d, 2H, *J* = 4.9 Hz), 5.08 (s large, 1H, OH), 5.25 (m, 2H,), 5.38 (d, 1H, *J* = 18,0 Hz), 6.07 (ddd, 1H, *J* = 5.5, 10.6, 18.0 Hz), 6.52 (s, 2H), 6.72 (d, 2H, *J* = 17.7 Hz), 6.85 (m, 3H). ^{13}C NMR ($CDCl_3$, 125 MHz) □ 14.5, 18.1, 20.1, 22.8, 23.5, 26.0, 27.6, 28.5, 37.9, 38.6, 47.0, 70.7, 77.2, 78.4, 106.4 (2 C), 110.7, 112.7, 117.6, 121.4, 121.7 (2 C), 123.2, 125.9, 128.9, 134.2, 135.6, 137.8, 144.3, 148.1, 155.3 (2 C). HRMS (ESI): *m/z* calculated for $C_{32}H_{41}O_5$+ [M+H]$^+$: 505.2954. found: 505.2948. $[\alpha]_D^{21}$ (*c* 0.2, CHCl3) = +47°.

5-((*E*)-2-((7a*R*,9*R*,11a*R*)-9-hydroxy-8,8,11a-trimethyl-2,7,7a,8,9,10,11,11a-octahydropyrano[3,2-c] xanthen-5-yl) vinyl)-2-(3-methylbut-2-en-1-yl) benzene-1,3-diol (**10**). Following procedure B, compound **10** (37 mg) was obtained with 37% yield from compound **8** (97 mg). ^{1}H NMR ($CDCl_3$. 500 MHz) □ 0.86 (s, 3H), 1.09 (s, 3H), 1.22 (s, 3H), 1.59 (m, 1H), 1.69 (dd, 1H, *J* = 6.7 and 11.5 Hz), 1.74 (s, 3H), 1.80 (m, 1H), 1.81 (s, 3H), 1.84 (m, 1H), 2.10 (m, 1H), 2.71 (m, 1H), 3.40 (m, 1H), 3.42 (m, 1H), 4.76 (ddd, 2H, *J* = 3.1, 14.6, 27.6 Hz), 5.25 (t, 1H, *J* = 6.6 Hz), 5.82 (m, 1H), 6.52 (s, 2H), 6.67 (d, 1H, *J* = 16 Hz), 6.73 (d, 1H, *J* =

10.3 Hz), 6.89 (s, 1H), 7.13 (d, 1H, *J* = 16Hz). ^{13}C NMR ($CDCl_3$, 125 MHz) □ 14.5, 18.1, 20.4, 22.8, 23.7, 26.0, 27.6, 28.6, 38.0, 38.7, 47.1, 65.1, 74.4, 78.2, 78.4, 106.5 (2 C), 113.3, 119.2, 119.7, 121.2, 121.6, 122.3, 123.6, 125.1, 125.7, 129.1, 137.5, 141.6, 143.0, 155.4 (2 C). HRMS (ESI): *m/z* calculated for $C_{32}H_{39}O_5^+$ $[M+H]^+$: 503.2797; found : 503.2781; $[\alpha]_D^{21}$ (*c* 0.14, $CHCl_3$) = +21°.

(2*R*,4a*R*,9a*R*)-7-((*E*)-3,5-dihydroxy-4-(3-methylbut-2-en-1-yl) styryl)-1,1,4a-trimethyl-6-(3-methylbut-2-en-1-yl)-2,3,4,4a,9,9a-hexahydro-1H-xanthene-2,5-diol (**11**). Compound **9** (35 mg, 0.07 mmol) was heated at 150 °C in anhydrous DMF (0.8 mL) containing molecular sieves powder for 10h. The crude mixture was filtered, the residue was washed twice with acetone and the filtrate was concentrated in vacuo. The crude product was purified on preparative TLC plates of silica gel using heptane/AcOEt (3/7) to obtain compound **11** as a yellow oil (11 mg, 32%).^{1}H NMR ($CDCl_3$, 500 MHz) □ 0.87 (s, 3H), 1.09 (s, 3H), 1.23 (s, 3H), 1.62 (m, 1H), 1.71 (m, 1H), 1.75 (s, 3H), 1.77 (m, 1H), 1.85 (m, 1H) 1.82 (s, 3H), 1.87 (m, 1H), 2.01 (m, 1H), 2.70 (m, 2H), 3.40 (m, 2H), 3.44 (m, 1H), 3.50 (m, 2H), 4.98 (m, 2H), 5.17 (s large, 1H, OH), 5.25 (t, 1H, J = 6.6 Hz), 5.52 (s, 1H, OH), 5.96 (m, 1H), 6.51(s, 2H), 6.76 (d, 1H, *J* = 16 Hz), 6.92 (s, 1H), 7.21 (d, 1H, *J* = 16 Hz). ^{13}C NMR ($CDCl_3$, 125 MHz) □ 14.5, 18.1, 20.4, 22.8, 22.9, 26.0, 27.6, 28.4, 29.9, 37.9, 38.7, 47.5, 77.8, 78.2, 106.5 (2 C), 112.9, 115.1, 117.5, 120.5, 121.7, 126.7, 127.9, 129.2 (2 C), 135.5, 136.7, 137.8, 139.9, 143.0, 155.3 (2 C). HRMS (ESI): *m/z* calculated for $C_{32}H_{41}O_5^+$ $[M+H]^+$: 505.2954; found : 505.3015; $[\alpha]_D^{21}$ (*c* 0.25, $CHCl_3$) = +30°.

(2*R*,4a*R*,9a*R*)-5-hydroxy-7-((*E*)-2-(5-hydroxy-2,2-dimethylchroman-7-yl) vinyl)-1,1,4a-trimethyl-2,3,4,4a,9,9a-hexahydro-1H-xanthen-2-yl formate (**12**). Following procedure C, compound **12** (430 mg) was obtained with 64% yield from SW-G **2** (1670 mg). ^{1}H NMR ($CDCl_3$, 500 MHz) □ 0.96 (s, 3H), 1,01 (s, 3H), 1.24 (s, 3H), 1.32 (s, 6H), 1.66 (m, 1H), 1.79 (m, 3H), 1.84 (m, 1H), 1.96 (m, 1H), 2,03 (m, 1H), 2.64 (t, H, *J* = 6.8 Hz), 2.71 (m, 2H), 4.76 (dd, 1H, *J* = 4.6 and 11.1 Hz), 6.45 (s, 1H), 6.54 (s, 1H), 6.71 (s, 1H), 6.75 (d, 1H, *J* = 16.3 Hz), 6.84 (d, 1H, *J* = 16.3 Hz), 6.90 (s, 1H), 8.14 (s, 1H). ^{13}C NMR ($CDCl_3$, 125 MHz)□□ 15.6, 17.2, 20.4, 22.8, 24.9, 26.9 (2 C), 27.4, 32.4, 37.5, 37.6, 47.5, 74.3, 77.6, 79.5, 104.4, 107.9, 108.0, 110.0, 119.7, 121.9, 126.7, 128.4, 130.2, 137.3, 140.1, 145.4, 154.3, 155.3, 161.0. HRMS (ESI): *m/z* calculated for $C_{30}H_{37}O_6^+$ $[M+H]^+$: 493.2590; found: 493.2567; $[\alpha]_D^{21}$ (*c* 0.1, $CHCl_3$) = +38°.

(2*R*,4a*R*,9a*R*)-7-((*E*)-2-(5-hydroxy-2,2-dimethylchroman-7-yl)vinyl)-5-methoxy-1,1,4a-trimethyl-2,3,4,4a,9,9a-hexahydro-1H-xanthen-2-yl formate (**13**). Following procedure C, compound **13** (18 mg) was obtained with 56% yield from SW-F **3** (30 mg). ^{1}H NMR (CD_3CN, 500 MHz): □ 0.96 (s, 3H), 1,00 (s, 3H), 1.21 (s, 3H), 1.29(s, 6H), 1.72 (m, 1H), 1.78 (m, 4H), 1.86 (m, 1H), 2,02 (m, 1H), 2.60 (t, 2H, *J* = 6.8

Hz), 2.72 (m, 2H), 3.80 (s, 3H), 4.74 (dd, 1H, *J* = 3.6, 10.8 Hz), 6.46 (s, 1H), 6.51 (s, 1H), 6.85 (s, 1H), 6.87 (d, 1H, *J* = 16.3 Hz), 6.95 (d, 1H, *J* = 16.3 Hz), 6.97 (s, 1H); ^{13}C NMR (CD_3CN, 125 MHz) 15.8, 18.0, 20.3, 23.7, 25.7, 26.9 (2 C), 27.4, 32.9, 38.2, 38.3, 47.7, 56.4, 74.8, 77.4, 80.1, 104.9, 107.6, 108.2, 109.4, 121.7, 123.8, 127.3, 129.0, 130.3, 138.0, 143.5, 150.1, 156.2, 156.4, 162.3. HRMS (ESI): *m/z* calculated for $C_{31}H_{39}O_6^+$ $[M+H]^+$: 507.2747; found: 507.2736; $[\alpha]_D^{21}$ (*c* 1.0, $CHCl_3$) = +68°.

(2*S*,3*R*,4a*R*,9a*R*)-3-hydroxy-7-((*E*)-2-(5-hydroxy-2,2-dimethylchroman-7-yl)vinyl)-5-methoxy-1,1,4a-trimethyl-2,3,4,4a,9,9a-hexahydro-1H-xanthen-2-yl formate (**14**). Following procedure C, compound **14** (8 mg) was obtained with 23% yield from SW-E **4** (31 mg). ^{1}H NMR ($CDCl_3$, 500 MHz) 1.02 (s, 3H), 1.15 (s, 3H), 1.33 (s, 6H), 1.42 (s, 3H), 1.80 (t, 2H, *J* = 6.8 Hz), 1.90 (dd, 1H, *J* = 6.1, 12.0 Hz), 2.20 (dd, 1H, *J* = 3.7, 15.3 Hz), 2.45 (dd, 1H, *J* = 3.2, 15.3 Hz), 2.64 (t, 2H, *J* = 6.8 Hz), 2.77 (m, 2H), 3.86 (s, 3H), 4.89 (d, 1H, *J* = 3.4 Hz), 5.64 (dd, 1H, *J* = 3.0, 6.5 Hz), 6.45 (s, 1H), 6.56 (s, 1H), 6.75 (d, 1H, J = 16.7 Hz), 6.79 (s, 1H), 6.84 (s, 1H), 6.88 (d, 1H, *J* = 16.7 Hz), 8.06 (s, 1H), 8.10 (s, 1H).^{13}C NMR ($CDCl_3$, 125 MHz) .7, 17.2, 21.3, 23.0, 26.9 (2C), 28.7, 32.4, 37.5, 41.4, 47.3, 56.3,68.9 74.3, 75.9, 76.7, 104.4, 107.6, 107.9, 108.1, 120.6, 122.5, 12.6, 128.4, 129.7, 137.2, 142.0, 149.3, 154.3, 155.3, 160.2, 160.5; HRMS (ESI): *m/z* calculated for $C_{32}H_{39}O_8^+$ $[M+H]^+$: 551.2645; found: 551.2624; $[\alpha]_D^{21}$ (*c* 0.6, $CHCl_3$) = -41°.

(2*R*,4a*R*,9a*R*)-7-((*E*)-2-(5-hydroxy-2,2-dimethylchroman-7-yl) vinyl)-1,1,4a-trimethyl-2,3,4,4a,9,9a-hexahydro-1H-xanthene-2,5-diol (**15**). Following procedure E, compound **15** (36 mg) was obtained with 62% yield from compound **12** (61 mg). ^{1}H NMR ($CDCl_3$, 500 MHz) 0.86 (s, 3H), 1.09 (s, 3H), 1.21 (s, 3H), 1.32 (s, 9H), 1.60 (m, 1H), 1.69 (dd, 1H, *J* = 5.7 and 12.3 Hz), 1.76 (m, 1H), 1.79 (t, 2H, *J* = 6.6 Hz), 1.85 (m, 1H), 2.00 (s, 1H), 2.64 (t, 2H, *J* = 6.6 Hz), 2.69 (m, 2H), 3.41 (dd, 1H, *J* = 4.2 and 11.2 Hz), 6.45 (s, 1H), 6.54 (s, 1H), 6.70 (s, 1H), 6.73 (d, H, *J* = 16.6 Hz), 6.85 (d, 1H, *J* = 16.6 Hz), 6.89 (s, 1H). ^{13}C NMR ($CDCl_3$, 125 MHz)14.5, 17.2, 20.4, 23.0, 26.9 (2 C), 27.6, 28.4, 32.4, 37.8, 38.7, 47.5, 74.3, 78.1, 78.2, 104.3, 108.0 (2 C), 109.9, 119.7, 122.3, 126.6, 128.5, 130.0, 137.4, 140.2, 145.4, 154.2, 155.3. HRMS (ESI): *m/z* calculated for $C_{29}H_{37}O_5^+$ $[M+H]^+$: 465.2641; found: 465.2620; $[\alpha]_D^{21}$ (*c* 0.1, $CHCl_3$) = +9°.

(2*R*,4a*R*,9a*R*)-7-((*E*)-2-(5-hydroxy-2,2-dimethylchroman-7-yl)vinyl)-5-methoxy-1,1,4a-trimethyl-2,3,4,4a,9,9a-hexahydro-1H-xanthen-2-ol (**16**). Following procedure E, compound **16** (10 mg) was obtained with 53% yield from compound **13** (18 mg). ^{1}H NMR (CD_3CN, 500 MHz) 0.83 (s, 3H), 1.04 (s, 3H), 1.18 (s, 3H), 1.29 (s, 6H), 1.58b (m, 1H), 1.64 (t, 1H, *J* = 9.7 Hz), 1.70 (m, 1H), 1.74 (m, 1H), 1.78 (t, 1H, J = 7.0 Hz), 1.96 (m, 1H), 2.60 (t, 2H, *J* = 7.0 Hz), 2.71 (m, 2H), 3.32 (d, 1H), 3.80 (s, 3H), 6.44 (s, 1H), 6.51 (s, 1H), 6.84 (s, 1H), 6.86 (d, 1H, *J* = 16.7 Hz), 6.95 (d, 1H, *J* = 16.7 Hz), 6.95 (s, 1H). ^{13}C NMR (CD_3CN,

125 MHz) □ 14.9, 18.0, 20.4, 23.9, 26.9, 27.0, 27.8, 29.1, 32.9, 38.8, 39.2, 47.9, 56.4, 74.9, 78.0, 78.1, 104.9, 107.7, 108.1, 109.4, 121.9, 124.2, 127.1, 129.0, 130.1, 138.1, 143.8, 150.1, 156.2, 156.4. HRMS (ESI): *m/z* calculated for $C_{30}H_{39}O_5^+$ $[M+H]^+$: 479.2797; found: 479.2778; $[\alpha]_D^{21}$ (*c* 0.8, $CHCl_3$) = +18°.

(2*S*,3*R*,4a*R*,9a*R*)-7-((*E*)-2-(5-hydroxy-2,2-dimethylchroman -7-yl) vinyl)-5-methoxy-1,1,4a-trimethyl-2,3,4,4a,9,9a-hexahydro-1H-xanthene-2,3-diol (**17**). Following procedure E, compound **17** (5 mg) was obtained with 26% yield from compound **14** (20 mg). ^{1}H NMR (CD_3CN, 500 MHz) □ 1.02 (s, 3H), 1.05 (s, 3H), 1.29 (s, 6H), 1.35 (s, 3H), 1.72 (m, 1H), 1.77 (t, 2H, *J* = 6.8 Hz), 1.88 (dd, 1H, *J* = 3.2, 14.0 Hz), 2.26 (dd, 1H, *J* = 2.8, 14.0 Hz), 2.60 (t, 2H, *J* = 6.8 Hz), 2.75 (m, 2H), 2.97 (m, OH), 3.28 (m, 1H), 3.80 (s, 3H), 4.10 (m, 1H), 6.44 (s, 1H), 6.51 (s, 1H), 6.86 (s, 1H), 6.87 (d, 1H, *J* = 6.8 Hz), 6.97 (s, 1H) 6.97, (d, 1H, *J* = 16 Hz); 13C NMR (CD_3CN, 125 MHz) □ 16.6, 18.0, 22.1, 23.8, 27.0 (2 C), 29.3, 33.0, 38.9, 44.4, 48.0, 56.4, 71.5, 74.9, 77.7, 78.0, 104.9, 107.6, 108.2, 109.4, 121.8, 124.4, 127.1, 129.0, 130.0, 138.0, 143.4, 150.2, 156.2, 156.4. HRMS (ESI): *m/z* calculated for $C_{30}H_{39}O_6^+$ $[M+H]^+$: 495.2747; found: 495.2727; $[\alpha]_D^{21}$ (*c* 0.5, $CHCl_3$) = +20°.

(2*R*,4a*R*,9a*R*)-5-hydroxy-7-(2-(5-hydroxy-2,2-dimethylchroman-7-yl)ethyl)-1,1,4a-trimethyl-2,3,4,4a,9,9a-hexahydro-1H-xanthen-2-yl formate (**18**). Following procedure D, compound **18** (201 mg) was obtained with 38% yield from SW-G **2** (500 mg). ^{1}H NMR ($CDCl_3$, 500 MHz) □□0.95 (s, 3H), 0.99 (s, 3H), 1.23 (s, 3H), 1.31 (s, 6H), 1.67 (m, 1H), 1.70 (m, 1H), 1.78 (t, 2H, *J* = 6.8 Hz), 1.85 (m, 1H), 1.94 (m, 1H), 2.02 (m, 1H), 2.61 (t, 2H, *J* = 6.8 Hz), 2.66 (m, 2H), 2.67 (s, 4H), 4.76 (dd, 1H, *J* = 4.2 and 11.7 Hz), 6.19 (s, 1H), 6.28 (s, 1H), 6.44 (s, 1H), 6.61 (s, 1H), 8.12 (s, 1H); ^{13}C NMR ($CDCl_3$, 125 MHz) □ 15.6, 17.0, 20.3, 22.8, 25.0, 26.9 (2 C), 27.4, 32.5, 37.3, 37.6, 37.7, 38.0, 47.6, 74.1, 77.1, 79.6, 106.1, 106.5, 109.7, 112.4, 120.2, 121.6, 134.3, 138.2, 141.8, 145.1, 154.0, 155.0, 161.0. HRMS (ESI): *m/z* calculated for $C_{30}H_{39}O_6^+$ $[M+H]^+$: 495.6360; found: 495.2743; $[\alpha]_D^{21}$ (*c* 0.7, $CHCl_3$) = +48°.

(2*R*,4a*R*,9a*R*)-7-(2-(5-hydroxy-2,2-dimethylchroman-7-yl)ethyl)-5-methoxy-1,1,4a-trimethyl-2,3,4,4a,9,9a-hexahydro-1H-xanthen-2-yl formate (**19**). Following procedure D, compound **19** (128 mg) was obtained with 33% yield from SW-F **3** (368 mg) .^{1}H NMR ($CDCl_3$, 500 MHz) □□0.94 (s, 3H), 0.98 (s, 3H), 1.24 (s, 3H), 1.31 (s, 6H), 1.67 (m, 1H), 1.70 (m, 1H), 1.78 (t, 2H, *J* = 6.8 Hz), 1.85 (m, 1H), 1.94 (m, 1H), 2.02 (m, 1H), 2.61 (t, 2H, *J* = 6.8 Hz), 2.66 (d, 2H, *J* = 8.9 Hz), 2.73 (m, 4H), 3.78 (s, 3H), 4.76 (dd, 1H, *J* = 4.3 and 11.5 Hz), 6.18 (s, 1H), 6.28 (s, 1H), 6.49 (s, 1H), 6.51 (s, 1H), 8.11 (s, 1H). ^{13}C NMR ($CDCl_3$, 125 MHz) □ 15.6, 17.0, 20.0, 23.2, 25.1, 26.9 (2 C), 27.5, 32.5, 37.5, 37.6, 38.1, 38.2, 47.2, 56.2, 74.1, 76.3,

79.8, 106.1, 106.6, 109.8, 110.1, 121.2, 122.2, 133.5, 140.8, 141.9, 148.8, 154.0, 155.0, 161.0. HRMS (ESI): *m/z* calculated for $C_{31}H_{41}O_6^+$ $[M+H]^+$: 509.2903; found: 509.2904; $[\alpha]_D^{21}$ (*c* 1.0, $CHCl_3$) = +31°

(2*R*,4a*R*,9a*R*)-7-(2-(5-hydroxy-2,2-dimethylchroman-7-yl)ethyl)-1,1,4a-trimethyl-2,3,4,4a,9,9a-hexahydro-1H-xanthene-2,5-diol (**20**). Following procedure E, compound **20** (12 mg) was obtained with 49% yield from compound **18** (25 mg). ^{1}H NMR ($CDCl_3$, 500 MHz) 0.87 (s, 3H), 1.1 (s, 3H), 1.20 (s, 3H), 1.31 (s, 6H), 1.60 (m, 1H), 1.67 (dd, 1H, *J* = 5.5, 11.6 Hz), 1.75 (m, 1H), 1.78 (t, 2H, *J* = 7.0 Hz), 1.85 (m, 1H), 2.00 (m, 1H), 2.61 (t, 2H, *J* = 6.8 Hz), 2.66 (m, 2H), 2.70 (s, 4H), 3.41 (dd, 1H, *J* = 4.2 and 11.9 Hz), 6.19 (s, 1H), 6.29 (s, 1H), 6.44 (s, 1H), 6.59 (s, 1H). ^{13}C NMR ($CDCl_3$, 125 MHz) 14.5, 17.0, 20.3, 22.9, 26.9 (2 C), 27.6, 28.4, 32.5, 37.3, 38.0, 38.1, 38.7, 47.7, 74.4, 77.6, 78.3, 106.1, 106.5, 109.7, 112.3, 120.2, 122.0, 134.1, 138.4, 141.9, 145.0, 154.0, 155.0. HRMS (ESI): *m/z* calculated for $C_{29}H_{39}O_5^+$ $[M+H]^+$: 467.2797; found: 467.2716; $[\alpha]_D^{21}$ (*c* 0.2, $CHCl_3$) = +28°.

(2*R*,4a*R*,9a*R*)-7-(2-(5-hydroxy-2,2-dimethylchroman-7-yl)ethyl)-5-methoxy-1,1,4a-trimethyl-2,3,4,4a,9,9a-hexahydro-1H-xanthen-2-ol (**21**). Following procedure E, compound **21** (12 mg) was obtained with 61% yield from compound **19** (20 mg). ^{1}H NMR ($CDCl_3$, 500 MHz) 0.85 (s, 3H), 1.07 (s, 3H), 1.21 (s, 3H), 1.31 (s, 6H), 1.59 (m, 1H), 1.67 (t, 1H, *J* = 8.9 Hz), 1.78 (t, 2H, *J* = 6.6 Hz), 1.80 (m, 1H), 1.83 (m, 1H), 2.09 (m, 1H), 2.61 (t, 2H, *J* = 6.6 Hz), 2.66 (d, 2H, *J* = 8.9 Hz), 2.71 (m, 4H), 2.74 (m, 2H), 3.41 (dd, 1H, *J* = 3.8 and 11.5 Hz), 3.78 (s, 3H), 6.17 (s, 1H), 6.29 (s, 1H), 6.49 (s, 1H), 6.51 (s, 1H). ^{13}C NMR ($CDCl_3$, 125 MHz) 14.5, 17.0, 20.1, 23.3, 26.8 (2 C), 27.8, 28.5, 32.5, 37.5, 38.0, 38.1, 38.6, 47.0, 56.2, 74.2, 76.8, 78.6, 106.1, 106.6, 109.7, 109.9, 121.2, 122.6, 133.3, 140.9, 141.9, 148.7, 154.0, 155.0. HRMS (ESI): *m/z* calculated for $C_{30}H_{41}O_5^+$ $[M+H]^+$: 481.2954; found: 481.2879; $[\alpha]_D^{21}$ (*c* 1.0, $CHCl_3$) = +25°.

Protein expression and purification. The human OSBP ORD fragment (401-807) with a C-terminal 6×His tag was purified from baculovirus-infected Sf9 cells. For experimental details, see ref. 16

Sterol transfer assay. For experimental details see ref.16. Data analysis: The signal was first corrected from compounds intrinsic fluorescence, then curves were fitted either with a linear equation (for slow kinetics) or, for fast kinetics, with an exponential equation $\Delta F = \Delta F_{max}(1 - e^{-kt})$, to determine the apparent kinetic constant, k. The apparent kinetic constant (k) obtained for each kinetic was then plotted against the concentration of the drugs. From this representation, we determined the inhibition constant Ki for each compound. We use two types of equations:

- For compounds with a strong affinity for ORD, the concentration of free compound cannot be approximated to the total concentration of the compound [I]. Therefore, the inhibition curve was fitted with a quadratic equation:

$$k = k_{max}(1 - \frac{[I] + K + [ORD] - \sqrt{([I] + K + [ORD])^2 - 4[I][ORD]}}{2[ORD]})$$

- For compounds with a low affinity for ORD, we used a hyperbolic function because the free drug concentration can be assumed to be identical to the total concentration [I]:

$$k = k_{max}\left(1 - \frac{[I]}{[I] + K}\right)$$

Cell culture and proliferation assay. Cancer cell lines were obtained from the American Type Culture Collection (Rockville, MD, USA) and were cultured according to the supplier's instructions. Human A549 lung cancer cells were grown in RPMI 1640 supplemented with 10% fetal calf serum (FCS) and 1% glutamine. Human U-87MG glioblastoma cells were grown in DMEM supplemented with 10% FCS and 1% glutamine. Cell lines were maintained at 37 °C in a humidified atmosphere containing 5% CO_2. Cells were seeded at 3000 cells/well density into white wall 96-well plates and then treated on the following day with the drugs. After 72 h treatment, cell viability was measured using CellTiter-Glo Luminescent Cell Viability Assay (Promega) and the luminescence was detected in a FLUOstar Omega microplate reader (BMG Labtech). The viability values of DMSO-treated cells were considered as 100%, then surviving curves and IC_{50} values were determined using GraphPad Prism 7.0 software.

Cell microscopy. For immunofluorescence, hTERT-RPE-1 cells cultured on µ-slides (Ibidi) were washed once with PBS then fixed with paraformaldehyde (4%) and glutaraldehyde (0.1%) in PBS for 10 min. Fixed cells were soaked in PBS supplemented with NH_4Cl (50 mM) for 10 min and then permeabilized in permeabilization buffer (Saponin 0.05 %, BSA 0.2 %, PBS) for 30 min at r.t.. Cells were then immuno-labeled with primary antibodies (diluted in permeabilization buffer) for 1 h at r.t., washed 3 times with permeabilization buffer, further incubated with secondary Alexa Fluor-conjugated antibodies (diluted in permeabilization buffer) for 30 min at r.t., and rinsed in PBS. For protein expression, cells were transfected with GFP-P4M^{SidM} and TagBFP-βGalT1 by electroporation using the Amaxa Nucleofector device (Lonza) and plated in µ-Dish 35 mm (Ibidi) for 18 to 24 h. Widefield microscopy was performed using an Olympus IX83 inverted microscope equipped with a Z-drift compensator, a scanning stage SCAN IM (Märzhäuser), an iXon3 blue-optimized EMCCD camera (Andor), and an UPlanSApo 60X/1.35 Oil

objective (Olympus). Compounds **2** and **12** were imaged using Semrock BrightLine filters (320/40 nm band-pass filter, 347 nm dichroic beam splitter, and 390/40 nm band-pass filter). For timelapse microscopy, Ibidi dishes were mounted in a stage chamber set at 37 °C (Okolab). Confocal microscopy was performed with a Zeiss LSM 780 microscope operated with ZEN software using a Plan-Apochromat 63X/1.4 Oil objective (Carl Zeiss).

Western blot analysis. Cells were seeded in 6-well plates and cultured as previously described for two days before each experiment. Cells were then harvested and lysed in RIPA buffer (50 mM Tris pH 8, 400 mM NaCl, 1% Triton-X-100, 0.5% sodium deoxycholate, 0.1% SDS) supplemented with EDTA-free protease inhibitor cocktail (Roche) on ice for 30 min. After 10 min of centrifugation (8,000 g), supernatant was collected and protein concentration was determined with the BCA pierce kit dosage. Protein extracts were mixed with 20% 5X Laemmli blue buffer and heated at 96 °C for 5 min. Then, clear lysates (5 µg) were run in 4-20% Mini-PROTEAN® TGX™ Precast Protein Gels (Biorad) transferred onto a PVDF membrane. The membranes were blocked with 5% w/v BSA in TBST, probed with antibodies against AKT (4691S), phospho-AKT (4060S), S6 (2217S), phospho-S6 (4856S), S6K (2708S), phospho-S6K (9205S), P62 (5114S) and LC3 AB (12741S) from Cell Signaling. Antibody against βactin (A5441) was obtained from Sigma. The secondary antibody HRP conjugated anti-mouse (P0447) was obtained from Dako and HRP conjugated anti-rabbit (7074) from Cell Signaling. Immunoreactivity was revealed using an enhanced chemoluminescence detection kit (Clarity™ Western ECL Substrate, Biorad) and visualized by Chemidocs imaging system, Image Lab software (V6.0.0). The band intensities were normalized to equal loading control β-actin.

***In vitro* mouse plasma stability**. Experiments were performed at 37 °C in male mouse plasma supplied by Biopredic (France). Reactions were initiated by the addition of a 5 µM solution of test compounds **2**, **12** or **15** to preheated plasma solution to yield a final concentration of 2.5 µM. Samples were collected at 0, 15, 30, 45, 60, and 120 min and acetonitrile was immediately added to stop the reaction. Samples were subjected to centrifugation for 10 min at 20,000 g at 4 °C and the clear supernatants were analyzed by LC-MS/MS with multiple reaction monitoring (MRM). All incubations were performed in duplicate. Procaine was used as the positive control. The MRM area response of the analyte for time = 0 (control) was set to 100%. The relative decrease in MRM area intensity over time against that of the control (percent parent decrease) was used to determine the half-life of elimination (t1/2) and the percentage of the remaining compound at 120 min. The UPLC−MS/MS system consisted of a Waters ACQUITY UPLC® System with an Acquity UPLC BEH RP18 1.7 µm, 2.1 x 50 mm column and a reversed phase gradient. Mobile phase A was 0.1% formic acid in water and mobile phase B 0.1% formic acid in

methanol coupled to a Waters XEVO™ TQ-S Mass Spectrometer operating in positive ion electrospray MRM mode. All solvents and chemicals were of LC/MS grade and were purchased from VWR International.

Metabolic stability in mouse microsomes. Compounds **2**, **12** or **15** (2.5 µM) were incubated in NADPH (1 mM) and 0.1 M, pH 7.4 phosphate buffer at 37 °C. After pre-warming the mixture for 5 min, reactions were initiated by the addition of 0.5 mg/mL of pooled male mouse microsomes (Biopredic, France). Samples were collected at 0, 5, 15, 30, 45 min and acetonitrile was immediately added to stop the reaction. Samples were centrifuged 10 min at 20,000 g at 4 °C and the supernatants were analyzed by LC-MS/MS with multiple reaction monitoring (MRM). All incubations were performed in duplicate. Diphenhydramine was used as the positive control. The MRM area response of the analyte for time = 0 (control) was set to 100%. The relative decrease in MRM area intensity over time against that of the control (percent parent decrease) was used to determine the half-life of elimination (t1/2) of compound in the incubation. Half-life values were calculated from the relationship: t (min) = 0.693/k, where k is the slope of the Ln concentration *vs.* time curve. The intrinsic clearance (Clint) was calculated as: Clint = (0.693 x incubation volume (µL))/(t (min) x mg of microsomal protein). Percentage of metabolism non-NADPH dependent was also monitored up to end-point incubation without NADPH.

Formulations of tested compounds. Compound **12** was dissolved in a vehicle (prepared with 15% final volume of hydroxypropyl-β-cyclodextrin in phosphate buffer 65 mM at pH 7.4) under fast (~700 rpm) magnetic stirring overnight, protected from light at room temperature. Once fully dissolved, the working solutions at 2, 2.5 or 5 mg/mL were stored at + 4°C protected from light. They could be used for one week of dosing. Temozolomide was dissolved in a vehicle made of 66.6% PBS1X, with 33.3% glucose 5% and 0.1% Tween 80 under magnetic stirring, then sonicated up to 40 minutes to obtain a homogeneous suspension. The working solutions at 4.2 mg/mL were stored at room temperature, protected from light, under continuous magnetic stirring, and used on the day of the preparation.

Estimation of the plasma concentrations of compounds 12 and 15. This early screening test was conducted to estimate plasma concentrations of compounds **12** and **15** after intraperitoneal single administration of compound **12** at two different doses, *i.e*., 5 mg/kg and 20 mg/kg. Six male Swiss mice, around 5-6 weeks old, supplied by Janvier Labs were used for the two experiments. Process, treatment and euthanasia were conducted according to the current procedures used at Eurofins | Adme bioanalyses who performed the assays. Briefly, 8 mL/kg and 2 mL/kg of a 2.5 mg/mL solution of compound **12** prepared according to the above protocol were injected intraperitoneally to a panel of

three mice. After 5 min, 15 min, 30 min, 1 h, 3 h and 6 h, about 0.07 mL blood was collected in the retro-orbital sinus of each mouse. Blood samples were centrifuged at 2000 g for five minutes at +4 °C to recover the plasma. For 20 µL of each plasma sample, 200 µL of acetonitrile were added to induce protein precipitation. Analysis of the supernatant was performed by a LC-MS/MS analysis, using an analytical method developed on the target molecules. Eight calibration standards were used to prepare the calibration curve in plasma with a calibration range between 1 and 2,000 ng/mL of plasma.

***In vivo* experiments.** These experiments were conducted to determine the antitumor activity of compound **12** at two different doses, *i.e.*, 20 mg/kg and 50 mg/kg (intraperitoneal administration) used as a single agent or in combination with temozolomide at 42 mg/kg (*per os* administration) in the GBM1-HAM patient-derived glioblastoma xenograft model (Xentech®), developed in immunodeficient female mice. Five-week athymic nude (*nu/nu*) female mice (*HSD: Athymic Nude-Foxn1^{nu}*), weighing 18-25 g, supplied by *ENVIGO* (Gannat, France), were used for these experiments. All experiments were performed by Xentech® in accordance with French legislation concerning the protection of laboratory animals and in accordance with a valid license for experiments on vertebrate animals issued by the French Ministry of Higher Education, Research and Innovation. APAFIS#19260-2019021311503803v1. Briefly, GBM1-HAM patient-derived tumours of the same passage were transplanted subcutaneously onto 3-24 mice (donor mice, passage (n-1)). When these tumours reached 1080 to 1688 mm^3, 5 donor mice were sacrificed by cervical dislocation. Tumours were aseptically excised and dissected. After removing necrotic areas, tumours were cut into fragments measuring approximately 20 mm^3 and transferred in a culture medium before grafting. 103 mice were anesthetized with 100 mg/kg ketamine hydrochloride and 10 mg/kg xylazine. The skin of anesthetized mice was disinfected with a chlorhexidine solution, incised on the interscapular region, and one 20 mm^3 tumour fragment was placed in the subcutaneous tissue. The skin was closed with clips. All mice from the same experiment were implanted on the same day. 50 mice with GBM1-HAM established growing tumours between 75 and 196 mm^3 were allocated in five groups. Each group initially included 10 mice: compound **12** vehicle at 10 mL/kg (daily intraperitoneal administration for 17 consecutive days); compound **12** at 50 mg/kg (daily intraperitoneal administration for 17 consecutive days); temozolomide at 42 mg/kg (daily *per os* administration for 5 consecutive days); compound **12** at 50 mg/kg (daily intraperitoneal administration for 27 consecutive days) in combination with temozolomide at 42 mg/kg (daily *per os* administration for 5 consecutive days); compound **12** at 20 mg/kg (daily intraperitoneal administration for 27 consecutive days) in combination with temozolomide at 42 mg/kg, (daily *per os* administration for 5 consecutive days). Treatments were initiated 11 days post-implantation of the tumor. The study was terminated

following 28 days after the start of treatment. Tumour volume was evaluated by measuring tumour diameters with a calliper three times a week during the treatment period. Recordings were expressed as mean ± standard error of the mean (m ± sem). Tumour growth curves were obtained by plotting the mean tumour volume in mm^3 against time for each experimental group. Delta tumour volumes (relative tumour volumes of the treated group compared to relative tumour volumes of the control group) were used for statistical analysis.

First estimation of blood barrier permeability. This early screening test was conducted to estimate plasma and brain concentrations of compound 15 obtained after intraperitoneal single administration of compound **12** (15 mg/kg) in male Swiss mice. Nine male Swiss mice around 5-6 weeks old supplied by Janvier Labs were used. Process, treatment and euthanasia were conducted according to the current procedures used at Eurofins | Adme bioanalyses who performed the assays. Briefly, 3.75 mL/kg of a solution of compound **12** (4 mg/mL) prepared according to the protocol described above was injected intraperitoneally to a panel of nine mice (*i.e.*, 15 mg/kg of compound **12**). After 0.25 h, 0.75 h and 1.5 h, the blood of three mice was collected. Blood samples were centrifuged at 2000 g for five minutes at +4°C for recovering plasma. After blood sampling, the animals were deeply anesthetized with Isoflurane and then perfused with 7 mL of saline solution directly into the heart to extract the maximal blood from the brain, after which they were sacrificed. 150 µL of acetonitrile was added to 50 µL of each plasma sample. After protein precipitation, analysis was performed using LC-MS/MS according to previous analytical test results. Brain samples were homogenized with an Ultra-turrax® using UHQ water (1:1, w/w). 50 µL of the homogenate was taken and 150 µL of acetonitrile was added. The mixture was vortex mixed for 60 s and centrifuged 5 min at 2000 rpm at 4 °C. Brain homogenate supernatant was directly measured by LC-MS/MS, according to previous analytical test results.

ASSOCIATED CONTENT

Supporting Information. ^{1}H and ^{13}C NMR spectra of compounds **8**-**21**. UPLC chromatogram and mass spectra of compound **12**. Molecular formula strings. The following files are available free of charge.

AUTHOR INFORMATION

Corresponding Author

fanny.roussi@cnrs.fr

bruno.antonny@cnrs.fr

Author Contributions

F.R., B.A., S.D., B.M., J.B, J.B and T.V. conceived and planned the experiments. G.J., C.R., C.G., D.K., J.P., L.A., M.L, V.C.P., D.T.M.H., A.L.N. and A.P. carried out the experiments. M.L, V.C.P., and D.T.M.H. contributed to supply raw materials. All authors discussed the results. F.R. wrote the manuscript with support from B.A., S.D. J. B. and B.M. ‡These authors contributed equally.

Funding Sources: This research was funded by a maturation program grant managed by SATT Paris-Saclay (ref CM2017-0045), two "Investissement d'Avenir" grants managed by Agence Nationale de la Recherche (UPSaclay ref. CDE-2019-002288 / IRE 2019-083 and CEBA, ANR-10-LABX-25-01).

ACKNOWLEDGMENT

The authors warmly thank Dr Mathieu Gutmann for fruitful discussions.

ABBREVIATIONS

CNS (central nervous system), DHE (dehydroergosterol), ER (endoplasmic reticulum), GBM (glioblastoma), HHX (hexahydroxanthene), LTPs (lipid-transfer proteins), NCI (National Cancer Institute), OSBP (oxysterol-binding protein), PI4P (phosphatidylinositol 4-phosphate), SWs (schweinfurthins), TGN (trans-Golgi network), TMZ (temozolomide).

(1) Koubek, E. J.; Weissenrieder, J. S.; Neighbors, J. D.; Hohl, R. J. Schweinfurthins: Lipid modulators with promising anti-cancer activity. *Lipids* **2018**, *8*, 767-784.

(2) Thoison, O.; Hnawia, E.; Guiéritte-Voegelein, F.; Sévenet, T. Vedelianin, a hexahydroxanthene Derivative isolated from *Macaranga vedeliana. Phytochemistry* **1992**, *31* (4), 1439-1442.

(3) Beutler, J. A.; Shoemaker, R. H.; Johnson, T.; Boyd, M. R. Cytotoxic geranyl stilbenes from *Macaranga schweinfurthii*. *J. Nat. Prod.* **1998**, *61* (12), 1509-1512.

(4) Beutler, J. A.; Jato, J.; Cragg, G. M.; Boyd, M. R. Schweinfurthin D, a cytotoxic stilbene from *Macaranga schweinfurthii*. *Nat. Prod. Lett.* **2000**, *14* (5), 399-404.

(5) Yoder, B. J.; Cao, S.; Norris, A.; Miller, J. S.; Ratovoson, F.; Razafitsalama, J.; Andriantsiferana, R.; Rasamison, V. E.; Kingston, D. G. I. Antiproliferative prenylated stilbenes and flavonoids from *Macaranga alnifolia* from the Madagascar Rainforest. *J. Nat. Prod.* **2007**, *70* (3), 342-346.

(6) Klausmeyer, P.; Van Que, N.; Jato, J.; McCloud, T. G.; Beutler, J. A. Schweinfurthins I and J from *Macaranga schweinfurthii*. *J. Nat. Prod.* **2010**, *73* (3), 479-481.

(7) Péresse, T.; Jézéquel, G.; Allard, P. M.; Pham, V. C.; Huong, D. T. M.; Blanchard, F.; Bignon, J.; Lévaique, H.; Wolfender, J. L.; Litaudon, M.; Roussi, F. Cytotoxic prenylated stilbenes isolated from *Macaranga tanarius*. *J. Nat. Prod.* **2017**, *80* (10), 2684-2691.

(8) Stevens, J. W.; Meyerholz, D. K.; Neighbors, J. D.; Morcuende, J. A. 5'-Methylschweinfurthin G reduces chondrosarcoma tumor growth. *J. Orthop. Res.* **2018**, 1283-1293

(9) Kokolus, K.M.; Haley, J. S.; Koubek, E. J.; Gowda, R.; Dinavahi, S. S.; Sharma, A.; Claxton, D. F.; Helm, K. F.; Drabick, J. J.; Robertson, G. P.; Neighbors, J. D.; Hohl, R. J.; Schell T. D. Schweinfurthin natural products induce regression of murine melanoma and pair with anti-PD-1 therapy to facilitate durable tumor immunity. *Oncoimmunology* **2019**, *8*, 2, e1539614.

(10) McCormick, J. L.; McKee, T.C.; Cardellina, J.H.; Leid, M.; Boyd, M. R. Cytotoxic triterpenes from a marine sponge, *Stelletta* sp. *J. Nat. Prod.* **1996**, *59,* 1047-1050.

(11) Pettit, G. R.; Inoue, M.; Kamano, Y.; Herald, D. L.; Arm, C.; Dufresne, C.; Christie, N. D.; Schmidt, J. M.; Doubek, D. L.; Krupa; T. S. Isolation and structure of the powerful cell growth inhibitor cephalostatin 1. *J. Am. Chem. Soc.* **1988**, *110*, 2006-2007.

(12) Kubo, S.; Mimaki, Y.; Terao, M.; Sashida, Y.; Nikaido, T. Ohmoto, T. Acylated cholestane glycosides from the bulbs of *Ornithogalum saudersiae*. *Phytochem.* **1992**, *31*, 3969-3973.

(13) Burgett, A. W. G.; Poulsen, T. B.; Wangkanont, K.; Anderson, D. R.; Kikuchi, C.; Shimada, K.; Okubo, S.; Fortner, K. C.; Mimaki, Y.; Kuroda, M.; Murphy, J. P.; Schwalb, D. J.; Petrella, E. C.; Cornella-Taracido, I.; Schirle, M.; Tallarico, J. A.; Shair, M. D. Natural Products reveal cancer cell dependence on oxysterol-binding proteins. *Nat. Chem. Biol.* **2011**, *7* (9), 639-647.

(14) Mesmin, B.; Antonny, B. The counterflow transport of sterols and PI4P. *Biochim Biophys Acta* **2016**, *1861*, 940-951.

(15) Mesmin, B.; Bigay, J.; Moser von Filseck, J.; Lacas-Gervais, S.; Drin, G.; Antonny, B. A Four-step cycle driven by PI(4)P hydrolysis directs sterol/PI(4)P exchange by the ER-Golgi tether OSBP. *Cell* **2013**, *155*, 830-843

(16) Mesmin, B.; Bigay, J.; Polidori, J.; Jamecna, D.; Lacs-Gervais, S.; Antonny, B. Sterol transfer, PI4P consumption, and control of membrane lipid order by endogenous OSBP, *EMBO J.* **2017**, *36*, 21, 3156-3174.

(17) Péresse, T.; Kovacs, D.; Subra, M.; Bigay, J.; Tsai, M. C.; Polidori, J.; Gautier, R.; Desrat, S.; Fleuriot, L.; Debayle, D.; Litaudon, M.; Pham, V. C.; Bignon, J.; Antonny, B.; Roussi, F.; Mesmin, B. Molecular and cellular dissection of the OSBP cycle through a fluorescent inhibitor. *J. Biol. Chem.* **2020**, *295*, 4277-4288.

(18) Bao, X.; Zheng, W.; Hata Sugi N.; Agarwala K. L.; Xu Q.; Wang Z.; Tendyke K.; Lee W.; Parent L.; Li W.; Cheng H.; Shen Y.; Taylor N.; Dezso Z.; Du H.; Kotake Y.; Zhao N.; Wang J.; Postema M.; Woodall-Jappe M. *et al.* Small molecule schweinfurthins selectively inhibit cancer cell proliferation and mTOR/AKT signaling by interfering with trans-Golgi-network trafficking. *Cancer Biol. Ther.* **2015**, *16*, 589-601.

(19) Harmalkar, D. S.; Mali, J. R.; Sivaraman, A.; Choi, Y.; Lee, K. Schweinfurthins A–Q: isolation, synthesis, and biochemical properties. *RSC Advances* **2018**, *8*, 21191-21209.

(20) Neighbors, J. D.; Salnikova, M. S.; Beutler, J. A.; Wiemer D. F. Synthesis and structure–activity studies of schweinfurthin B analogs: evidence for the importance of a D-ring hydrogen bond donor in expression of differential cytotoxicity. *Bioorg. Med. Chem.* **2006**, *14*, 1771-1784.

(21) Kodet, J. G.; Mente, N. R.; Kuder, C. H.; Beutler, J. A.; Hohl, R. J.; Wiemer, D. F. Structural analogues of schweinfurthin F: Probing the steric, electronic, and hydrophobic properties of the D-ring substructure. *Bioorg. Med. Chem.* **2010**, *18*, 1676-1683.

(22) Stockdale, D. P.; Beutler, J. A.; Wiemer, D. F. Synthesis of amide isosteres of schweinfurthin-based stilbenes. *Bioorg. Med. Chem.*, **2017**, *25*, 5483-5489.

(23) Stockdale, D. P.; Beutler, J. A.; Wiemer, D. F. Substitution of a triazole for the central olefin in biologically active stilbenes. *Bioorg. Med. Chem.*, **2022**, *75*, 128980.

(24) Allard, P.-M.; Péresse, T.; Bisson, J.; Gindro, K.; Marcourt, L.; Cuong, P. V.; Roussi, F.; Litaudon, M.; Wolfender, J.-L. Molecular networking & in-silico fragmentation: complementary tools for dereplication in natural products chemistry. *Anal. Chem.* **2016**, *88*, 3317-3323.

(25) Péresse, T.; Elie, N.; Touboul, D.; Pham, V. C.; Dumontet, V.; Roussi, F.; Litaudon, M.; Brunelle, A. Dual beam depth profiling and imaging with argon and bismuth clusters of prenylated stilbenes on glandular trichomes of *Macaranga vedeliana*. *Anal. Chem.* **2017**, *89* (17), 9247-9252.

(26) Topczewski, J. J.; Callahan, M. P.; Kodet, J. G.; Inbarasu, J. D.; Mente, N. R.; Beutler, J. A.; Wiemer, D. F. Relevance of the C-5 position to schweinfurthin induced cytotoxicity. *Bioorg. Med. Chem.* **2011**, *19*, 7570-7581.

(27) Lykakis, I. N.; Efe, C.; Gryparis, C.; Stratakis, M. $Ph_3PAuNTf_2$ as a superior catalyst for the selective synthesis of 2H-chromenes: application to the concise synthesis of benzopyran natural products. *Eur. J. Org. Chem.* **2011**, 2334-2338.

(28) Bochicchio, A.; Cefola, R.; Choppin, S.; Colobert, F.; Di Noia, M. A.; Funicello, M.; Hanquet, G.; Pisano, I.; Todisco, S.; Chiummiento. L. Selective Claisen rearrangement and iodination for the synthesis of polyoxygenated allyl phenol derivatives. *Tet. Lett.* **2016**, 57, 4053-4055.

(29) Liu, T.; Zeng, Y.; Zhang, H.; Wei, T.; Wu, X.; Li, N. Facile Pd-catalyzed chemoselective transfer hydrogenation of olefins using formic acid in water. *Tet. Lett.* **2016**, *57*, 4845-4849.

(30) Hammond, G. R. V.; Machner, M. P.; Balla, T. A novel probe for phosphatidylinositol 4-phosphate reveals multiple pools beyond the Golgi. *J. Cell Biol*. **2014**, *205*, 113-126.

(31) Deleyto-Seldas, N.; Efeyan, A. The mTOR-autophagy axis and the control of metabolism. *Front. Cell Dev. Biol.* **2021**, *9*, Article 655731.

(32) Thakur, A.; Faujdar, C.; Sharma, R.; Sharma, S.; Malik, B.; Nepali, K.; Liou; J. P. Glioblastoma: current status, emerging targets, and recent advances. *J. Med. Chem.* **2022**, *65*, 8596-8685.

(33) Armarego, W. L. F. Chai, C. L. L. in Purification of Laboratory Chemicals, Butterworth-Heinemann, Elsevier, Oxford, 7th edn, **2013**.